DEVELOPMENT OF ELECTRODES BASED ON YTTRIUM CHROMITES AND RARE EARTH DOPED HAFNIA FOR MHD GENERATOR APPLICATIONS*

D. D. Marchant and J. L. Bates
Pacific Northwest Laboratory
Richland, Washington

PNL-SA- 7620
CONF - 790640 - - 9

Abstract

Yttrium chromites are being studied as potential high temperature electrodes for MHD. Like lanthanum chromites, the doped yttrium chromites have similar high electrical conductivity, predominantly electronic over a wide temperature range; however, they do not form hydroscopic decomposition products, which cause gross structural degradation. In addition, they exhibit substantially improved resistance to electrochemical attack by slag/seed. The electrical conductivity, thermal diffusivity/conductivity, melting points, thermal expansion, vaporization and electrochemical corrosion for several yttrium chromite compositions are reported and compared with analogous lanthanum chromites.

Hafnium oxide containing rare earth additions are also being studied as potential high temperature MHD electrodes. The electrode compositions show a high resistance to electrochemical corrosion in slag/seed. Hafnia-rare earth-M_2O_3 oxides can be fabricated with sufficient room temperature electrical conductivity to make them candidates for ceramic-to-metal current leadouts. Electrochemical tests of ceramic current leadout:ceramic electrode couples have been conducted at high temperatures and with high current densities for long periods of time with little interaction between the electrodes and leadouts.

I. Introduction

Chromites have long been considered as candidate electrode materials for medium hot wall MHD generator channels[1-3] and have successfully operated in clean-fuel open-cycle MHD test channels. The most studied is Mg or Sr doped lanthanum chromite. These doped chromites have excellent electronic electrical conducivity with a small temperature dependence. However, lanthanum chromites are subject to loss of chromium at high temperatures, and to corrosion by coal slag and molten alkali salts. The loss of chromium leads to the formation of La_2O_3 which is hygroscopic, resulting in volume changes which cause catastrophic mechanical degradation of the electrode material. Doped yttrium chromites are electrically similar to lanthanum chromites, having predominantly electronic conductivity with a low temperature dependence. However, these yttrium chromites do not form analogous hygroscopic compounds even when tested for long periods of time at high temperature.

II. Preparation

A series of yttrium chromite compositions have been prepared† with additives of Sr, Mg, Ca and Al. The range of compositions investigated are shown in the following formula:

$$Y_x[(Sr, Mg \text{ or } Ca)_y Cr_z]_w Al_{1-w} O_3$$

where x = 0.95 to 1
y = 0.02 to 0.2
z = 0.8 to 1
w = 1 to 0.8.

The $YCrO_3$ compositions were fabricated by mixing nitrates of the respective components (Y, Mg, Cr, and Al) in an ethelene glycol-citric acid-water solution. The mixture was dried at 383K then calcined between 1073K and 1273K to form the oxide. The calcined materials were mixed in a shaker mill using plastic containers and plastic balls. The powders were dry pressed using 1/8 wt% polyvinyl alcohol as the binder. The pressed bars were sintered to closed porosity at temperatures between 1773 and 2023K in H_2/CO_2 atmospheres with a PO_2 of $<10^{-6}$Pa. The bars were then oxidized by firing in air at 1773K. The air oxidation changes the color of the bars from dark green to a brown-black.

The yttrium chromites were generally multiphase. The analysis of these phases determined using the quantitative x-ray energy dispersion microprobe analysis capabilities of the scanning electron microscope (SEM-EDX) are given in Table 1. Most of the magnesium was found as a second phase with the larger amounts of magnesium additions resulting in larger amounts of the magnesium rich phase. Most of the alumina added to the chromite remained substituted for chromium although an aluminum rich second phase was formed. Adding 50% Al to the chromite resulting in a granular second phase containing mostly yttria.

The general chemical formula used above to identify the compositions was written based on the total number of moles of each cation present in the original formulations. This simplified nomenclature does not imply that the formulation exists as a single phase since the present knowledge of the $YCrO_3$ phase systems does not allow the assignment of the correct chemical formulas phases and solubilities. It is assumed that since both $YCrO_3$ and $LaCrO_3$ are perovskite structures, the yttrium chromite have similar crystallographic structures as lanthanum chromite.[3] Therefore, O, Cr and Y excesses are unlikely without the development of second phases. Also acceptor ions (Mg^{2+}, Sr^{2+}, etc.) in an oxidizing atmosphere will increase the oxidation state of Cr^{+3} to maintain electrical neutrality with the consequent increase in electrical conductivity. The electrical conductivity, thermal expansion, thermal diffusivity/conductivity, melting points, vaporization rates and electrochemical corrosion rates have been measured for the yttrium chromites and compared with the lanthanum chromites.

*Prepared for the U.S. Department of Energy under Contract EY-76-C-06-1830
†A. T. Research, Vicky, Missouri

DISCLAIMER

Table 1. SEM-EDX Compositional Analysis of Six Yttrium on one Lanthanum Chromite Based Materials

Composition	Atom % of Cations						
	Mg	Al	Si	Ca	Cr	Y	La
$Y\ Mg_{0.05}Cr_{0.95}O_3$							
Overall	1	2	3	0.2	47	48	
Matrix		1	2	0.5	46	50	
Second Phase-granular (2% of Area)	1		1		15	13	
Grain Boundary Phase at Some Triple Points	71		3	3		94	
$Y_{0.95}Mg_{0.05}CrO_3$							
Overall	1	1	1	0.7	49	47	
Matrix		1	3	0.3	49	50	
Second Phase-granular (2-4% of Area)	62		2	0.2	19	18	
$Y\ Mg_{0.1}Cr_{0.9}O_3$							
Overall	4	1	1	0.2	44	49	
Matrix		2		0.3	36	61	
Impurity	78		1	0.1	10	11	
$Y\ Mg_{0.2}Cr_{0.8}O_3$							
Overall	14	1	0.2		38	47	
Matrix	2	2	1	0.3	45	51	
Second Phase-granular (20% of Area)	68		1	0.1	10	21	
$Y(Mg_{0.05}Cr_{0.95})_{0.75}Al_{0.25}O_3$							
Overall	2	14	1	1	35	47	
Matrix		13		0.2	36	50	
Second Phase-granular (10% of Area)		43			27	30	
$Y(Mg_{0.05}Cr_{0.95})_{0.5}Al_{0.5}O_3$							
Overall		13			28	59	
Matrix		17		0.5	30	53	
Second Phase Large Islands (30% of Area)		3		0.3	4	92	
Third Phase granular small (5% of Area)	58	5	0.6	0.1	13	23	
$La(Mg_{0.05}Cr_{0.95})O_3$							
Overall		5	3	1	40		50
Matrix		4	4	1	42		50
Second Phase (2-4% of Area along grain boundaries)		6	10	<1	13		70

Melting Point

The melting points were measured in an argon atmosphere using a "V" type electrically heated tungsten filament.[4] The system was calibrated using metals and ceramics with known melting points, i.e., Mo, Al_2O_3, Pt, Ni, Au and Cu. A micro-optical pyrometer was used to view the sample and to measure the melting temperature. Three or more measurements were made for each composition with a reproducibility of ±10K. The average values are listed in Table 2. The melting points of the yttrium chromites are generally lower by about 150K of the analogous lanthanum chromites.

Vaporization Loss

Samples of several compositions were exposed to a flowing atmosphere of N_2 containing 101Pa·O_2 and 10.13kPa·H_2O at atmospheric pressure. The measurements made at 2013K for up to 63 hours are listed in Table 2. Included in the table are corresponding data for a composition of $LaCrO_3$. The vaporization losses of the $YCrO_3$ is slightly higher than those of the lanthanum chromite.

Thermal Expansion

The thermal expansion was measured in air using a Al_2O_3 pushrod dilatometer with linear heating and cooling rates of 4 degrees per minute. The average thermal expansion coefficients for the

Table 2. Thermal Expansion Melting Point Corrosion Rates and Vaporization Rates of Several Yttrium Chromite Based Compositions

Composition	Melting Point K	Average Thermal Expansion Coefficient $(10^{-6}/K)$ 373-1675K	K_2SO_4 Chemical Corrosion Rate $\mu g/cm^2$ hr	Vaporization Weight Loss $\mu g/cm^2$ hr
$Y\ CrO_3$				6
$Y\ Mg_{0.05}Cr_{0.95}O_3$	2475	8.73	400	48
$Y_{0.95}Mg_{0.05}CrO_3$	2476	8.81	90	96
$Y(Mg_{0.05}Cr_{0.95})_{0.85}Al_{0.15}O_3$	2463	8.75	0.2	-
$Y(Mg_{0.05}Cr_{0.95})_{0.75}Al_{0.25}O_3$	2373	8.35	1000	-
$Y(Mg_{0.05}Cr_{0.95})_{0.5}Al_{0.5}O_3$	2386	8.60	500	61
$Y\ AlO_3$	2223	8.83	80	-
$Y\ Mg_{0.1}Cr_{0.9}O_3$	2392	8.75	40	-
$Y\ Mg_{0.2}Cr_{0.8}O_3$	2474	8.80	50	-
$Y_{0.9}Sr_{0.1}CrO_3$	2411	8.31	500	199
$Y_{0.8}Sr_{0.2}CrO_3$	2426	10.56	50	-
$Y_{0.9}Ca_{0.1}CrO_3$	2362	9.45	600	123
$Y_{0.8}Ca_{0.2}CrO_3$	2395	9.40	100	119
$La_{0.95}Mg_{0.05}CrO_3$	2595	8.75	400	136[4] 10-44

temperature ranges are shown in Table 2. The thermal expansion increases slightly with temperature and the curvature is essentially smooth with minor inflections around 520 and 850K. These inflections are much less than that found in the corresponding lanthanum chromite and are found on both heating and cooling.

Thermal Diffusivity/Conductivity

The thermal diffusivity was measured using a laser pulse technique in an argon atmosphere heated in a tungsten mesh furnace.[6] The thermal conductivity was calculated as the product of diffusivity, measured density corrected for temperature using measured thermal expansion data and heat capacity. The heat capacity was calculated using Kopp-Neuman theory of mixtures from known specific heat data for the individual oxide components. Both the thermal diffusivity and thermal conductivity are shown in Figure 1.

The thermal diffusivity and thermal conductivity values of the $YCrO_3$ are approximately the same as that reported for $LaCrO_3$.[6] The thermal diffusivities/conductivities vary significantly depending upon the microstructure making it difficult to resolve changes due to the composition variation.

Electrical Conductivity

Electrical conductivity was measured using a four probe technique. Direct electric current (current densities not exceeding 0.05 amp/cm^2) was passed through the rectangular or cylindrical shaped samples held at each end by two knife-edge supports. The electric potential drop across the sample was measured using two electrically floating voltage probes. Measurements were made in air on samples that were air oxidized to 1773K, Figure 2.

The electrical conductivities of the chromites containing Mg are greater than the undoped chromite, even though the magnesium was concentrated in a second phase. The electrical conductivities are similar to the analogous doped lanthanum chromite. No polarization was observed during the measurements indicating that most of the conduction was electronic. Reduced (green) yttrium chromite had an electrical conductivity about two orders of magnitude less than the oxidized chromite (black). The same reduction in electrical conductivity was found in lanthanum chromite.

Chemical and Electrochemical Corrosion

Both chemical and electrochemical corrosion tests were conducted on the yttria chromites to compare their relative resistance to corrosion. As an initial test, each composition was submersed

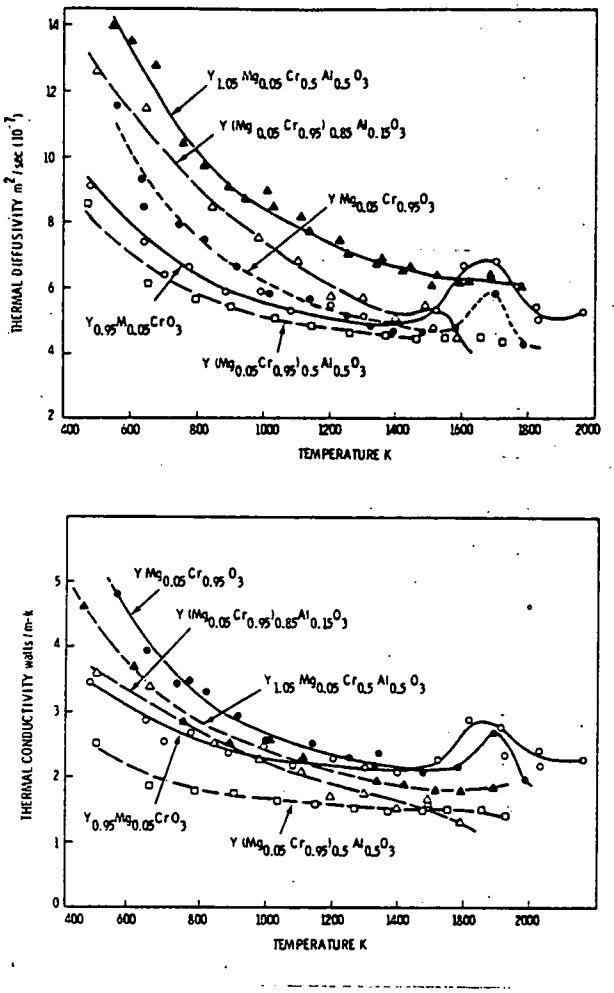

Figure 1. Thermal diffusivity and conductivity of several yttrium chromite compositions.

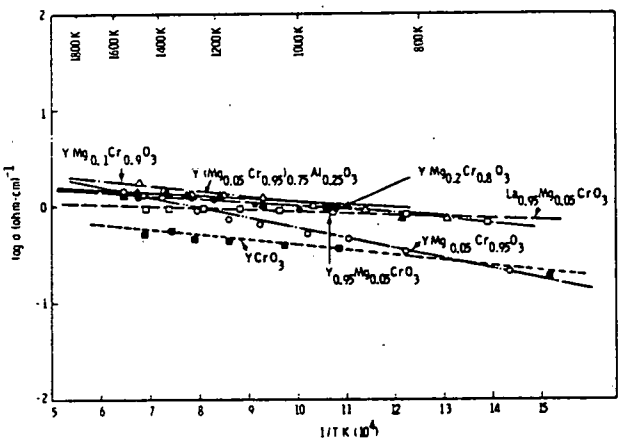

Figure 2. Electrical conductivity of several yttrium chromite compositions.

in K_2SO_4 at 1373K for 48 hrs and the corrosion rates determined from the weight changes, Table 2. Part of the wide fluctuation in corrosion rates are attributed to the microstructural differences which make comparisons difficult. The most promising compositions were chosen for further testing, i.e., $YMg_{0.05}Cr_{0.95}O_3$, $Y_{0.95}Mg_{0.05}CrO_3$ and $Y(Mg_{0.05}Cr_{0.95})_{0.85}Al_{0.15}O$, and $Y(Mg_{0.05}Cr_{0.95})_{0.75}Al_{0.25}O_3$. Comparison of the yttrium chromites with the analogous lanthanum chromite compositions and microstructures (Table 2) indicate that the yttrium chromite is more resistive to K_2SO_4 corrosion.

The advanced electrochemical tests of these selected compositions involved passing a direct electric current between two electrodes which were partially immersed in an electrolyte (synthetic molten coal slags or potassium salts). The basic test configuration included alumina sleeves around the chromite samples to channel current transport through the electrode end and a voltage probe equidistant from the anode and the cathode to measure the electric potential at the anode and cathode.

Tests were made in synthetic coal slag compositions containing 10 mole% K_2O to better simulate slag inside the MHD channel. The slag composition simulating Montana Rosebud (MR-1) is 42.4 wt% SiO_2, 18.8 wt% Al_2O_3, 12.9 wt% CaO, 6.9 wt% Fe_2O_3, 4.1 wt% MgO, 0.7 wt% TiO_2, 13.4 wt% K_2O, 0.4 wt% Na_2O, and 0.2 wt% P_2O_5. The slag composition simulating Illinois No. 6 (Ill #6-1) is 39.5 wt% SiO_2, 18.4 wt% Al_2O_3, 5.1 wt% CaO, 24.3 wt% Fe_2O_3, 1.6 wt% MgO, 0.8 wt% TiO_2, 11.7 wt% K_2O, 0.5 wt% Na_2O and 1 wt% P_2O_5.

A summary of the electrochemical tests on both yttrium and lanthanum chromites are shown in Table 3. The corrosion rates were determined by measuring the geometrical sample changes after mounting and polishing for ceramographic examination. This corrosion rate includes all material loss including that by grain boundary attack and resulting grain removal and by erosion and corrosion with the slag. The electrochemical corrosion rate for the tests where current has passed is expressed in μg/coul. In the simple corrosion tests where no current is passed, i.e., a control test, the corrosion rate is expressed as $\mu g/10^3$ sec. In those tests where a control was used, the corrosion rate of the control is much less (usually by at least an order of magnitude) than either the anode or cathode.

The lanthanum chromites generally degraded after testing in molten salts unless stored in a vacuum dessicator. The degradation is attributed to both potassium salt and lanthanum oxide hydration. The degradation also occurred in the vacuum dessicator after several weeks of storage. The yttrium chromites did not exhibit post test degradation, even after exposure to ambient air for up to five weeks.

The yttrium chromite is more resistant to electrochemical attack in both potassium seed and slag/seed than similar lanthanum chromites. The yttrium chromite tests were conducted for longer times than the lanthanum chromites with the lanthanum chromite tests often terminating due to sample failure. [The low corrosion rate for the $LaCrO_3$ (test 137) is attributed to very short testing time and resulting small amount of material

Table 3. Summary of Electrochemical Tests on Both Yttrium and Lanthanum Chromites

Test No.	Composition	Electrolyte	Temp, K	Time, S(10^3)	Current Density, Amp/cm^2	Anode	Corrosion, Rate, µg/coul Cathode	Control µg/10^{3}s
Yttrium Chromites								
160	Y $Mg_{0.05}Cr_{0.95}O_3$	K_2SO_4	1373	11.4	1.0	10	5-10	11.6
158	Y $Mg_{0.05}Cr_{0.95}O_3$	Ill#6-1	1723	17.1	0.8	7	14	11.6
162	Y $Mg_{0.05}Cr_{0.95}O_3$	MR-1	1723	66.7	0.7	111	80-95	
169	Y $Mg_{0.2}Cr_{0.8}O_3$	MR-1	1739	66.3	1.0	191	271	
167	Y $(Mg_{0.05}Cr_{0.95})_{0.75}Al_{0.25}O_3$	MR-1	1723	19.8	1.0	31	15	
170	Y $(Mg_{0.05}Cr_{0.95})_{0.85}Al_{0.15}O_3$	MR-1	1723	39.6	1.0	45	45	
198	$Y_{0.95}Mg_{0.05}CrO_3$	MR-1	1723	34.5	0.9	42	75	
Lanthanum Chromites								
6	$La_{0.95}Mg_{0.05}CrO_3$ (S)	K_2SO_4	1373	5	1.6	1014	315	
32	$LaMg_{0.05}Cr_{0.95}O_3$ (HP)	K_2SO_4	1373	3.6	1.6	-	652	
29	$LaMg_{0.05}Cr_{0.95}O_3$ (HP)	K_2SO_4	1373	1.1	1.0	289	-	
		K_2SO_4	1373	1.0	3.0	1094	-	
136	$La_{0.95}Mg_{0.05}CrO_3$ (HP)	Ill#6-1	1723	11	1.0	67	30	
137	$La_{0.95}Mg_{0.05}CrO_3$ (HP)	MR-1	1723	1.1	1.0	25-30	164	

removed.] Grain boundary penetration by potassium was significantly less in the yttrium chromites than in the lanthanum chromites.

Several types of corrosion mechanisms occurred during the electrochemical corrosion of both yttrium and lanthanum chromites. At the anode, gases are generated. These gases are O_2 and probably CO_2 and SO_2. The generation (possible cavitation) and movement of bubbles up the electrode surface resulted in additional erosion of the anode. Bubbles on the anode surface created electrically insulating zones, causing higher current densities in adjacent areas, and possibly higher corrosion in those areas free of bubbles.

In addition, the gas bubbles may have continually swept away corrosion products in the slag or on the anode surface, thus creating fresh surfaces and slag compositions for corrosion. In the MR-1 slag tests, even with slag migration, the electric potential between the platinum probe and the anode continually increased during the test indicating a decreasing conductivity of the slag. The low conductivity appears partially due to cation (Ca^{2+}, K^+, Na^+) migration away from the anode. This low conductivity may have forced the current to channel, increasing the possibility of arcing.

The platinum probe also measured cyclic voltage fluctuations of up to ±50% indicating bubble formation, current channelling, and possibly arcing. The resulting corrosion/erosion produced a uniformly shaped reaction zone. The Ill #6-1 slag tests exhibited lower voltage fluctuations and smaller electric potential increases at the anode. The anode electrochemical corrosion rates were less than in MR-1 slag. The anode in the Ill #6-1 slag also had a uniformly shaped reaction zone.

The electric potential fluctuations in both MR-1 and Ill #6-1 were much smaller (≤±5%) between the probe and the cathode than between the anode and probe since few bubbles were formed at the cathode. The conductivity of the slags near the cathode increased as cations (Ca^{2+}, K^+) are attracted to the cathode, consequently concentrating of current was not likely. In general, the cathode does not corrode uniformly like the anode and the electrochemical corrosion mechanisms are easier to identify since the reaction products remain close to the electrode.

In general, with electronically conducting electrodes, the degree of bubble formation at the anode will increase as the ionic transference of the slag increases. For example, the high iron containing Ill #6 slag has a higher conductivity and is more electronically conducting than the high calcium containing Montana "Rosebud" slag. Consequently, the bubble formation occurring in Ill #6 slag (test 158-Table 3) was significantly less than that observed in the "Rosebud" slag (test 198). In addition, the voltage fluctuation of test 158 did not exceed ±5%, suggesting little current bunching.

Tests 158 and 198 are representative of the interactions with Ill #6-1 and MR-1 slags, respectively. The electrode-reaction zone interface for both the anodes and cathodes of test 158 and 198 are shown in Figures 3 and 4, respectively. To better understand the electrochemical corrosion mechanisms, several anodes and cathodes were examined using the quantitative SEM-EDX. The details of the examinations are given elsewhere.[8,9] The chemical composition expressed as the atom% of the cations for the features identified as Figures 3 and 4 are given in Table 4.

The anodes remained relatively unchanged except at the immediate reaction interface, although the matrix did contain some Si contamination. Little grain boundary penetration of either slag or potassium occurred. At the reaction interface between the anode and slag the $YCrO_3$ dissolved with the formation of reaction products. This reaction zone consisted of discrete grains of reaction product surrounded by slag. In the high iron slag (Ill #6-1 test 158) the reaction products consisted of 1) an anode of Fe-Al-Cr (2:2:3) 2) metallic Fe and 3) single phase coal slag.

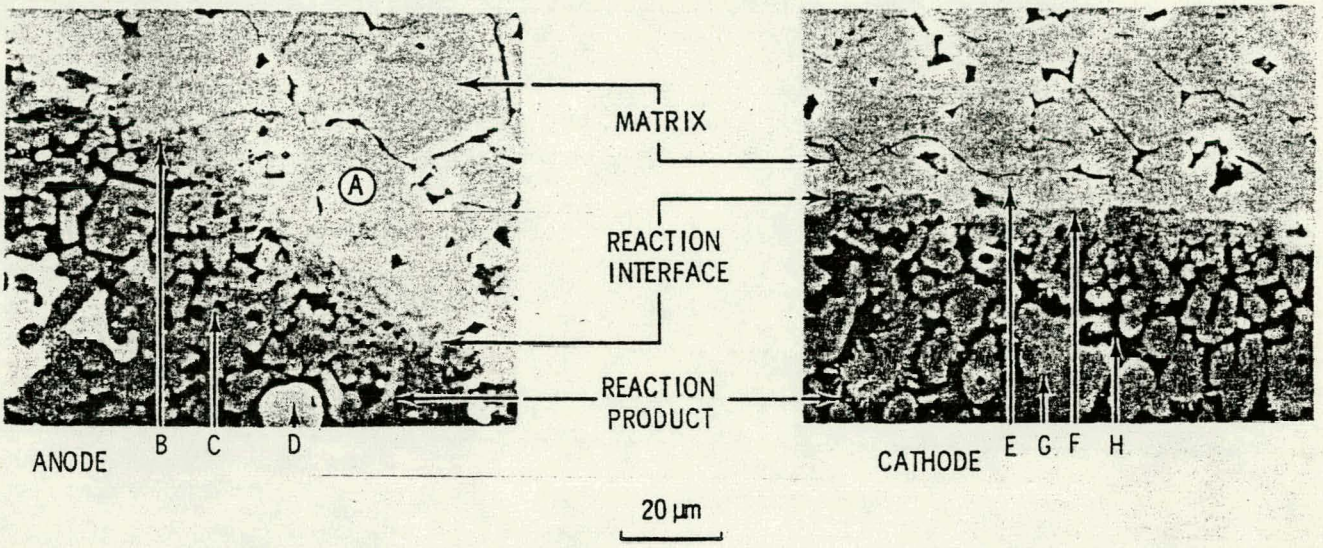

Figure 3. Microstructure of reaction zone Test 158

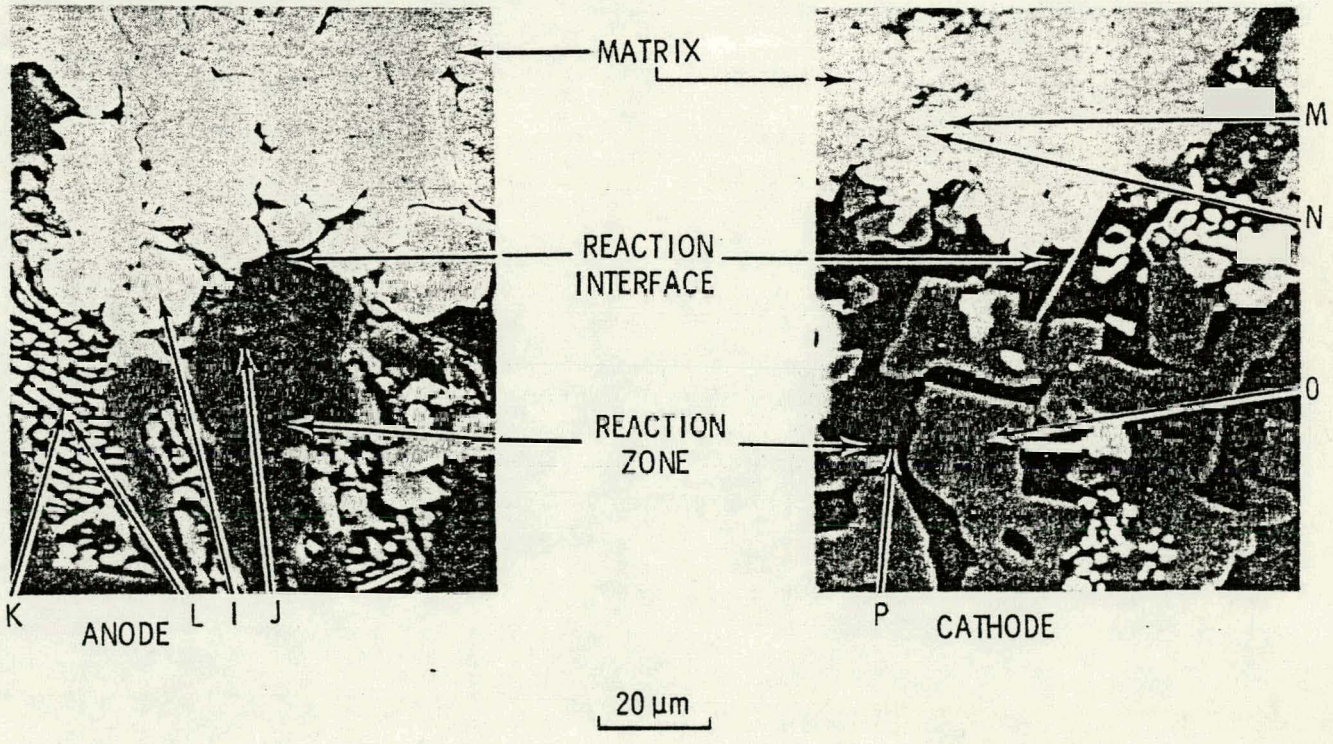

Figure 4. Microstructure of reaction zone for Test 198

Table 4. Compositions Determined by SEM-EDX of the Microstructural Features of Figures 1 and 2.

Feature	Descriptor	Atom % Mg	Al	Si	K	Ca	Ti	Cr	Fe	Y
Test 158 Anode (Figure 3)										
A	Matrix	2		4	0.2	0.7		43	0.5	51
B	Reaction Product at Reaction Interface	8	20	10	0.3	2	0.1	31	18	11
C	Reaction Product in Reaction Zone	9	26	3	0.3	0.3	0.1	38	24	0.1
D	Metallic Phase in Reaction Zone		2	3	0.3			2	93	0.3
Test 158 Cathode (Figure 3)										
E	Matrix	1	2	4	0.2	0.5	0.2	42	0.3	50
F	Reactor Product at Reaction Interface	2	23	6	0.2	2	0.3	24	19	23
G	Reaction Product in Reaction Zone	2	20	2	0.2	0.2	0.5	42	32	
H	Grain Boundary in Reaction Zone	3	26	44	9	3	0.4	6	7	1
Test 198 Anode (Figure 4)										
I	Matrix		3	2		0.7		42	0.7	51
J	Reaction Product in Reaction Zone		20	1		0.6	0.2	75	3	
K	Second Phase in Reaction Zone	2	9	43		2	0.3	1	1	42
L	Grain Boundary in Reaction Zone	9	24	34	0.2	6	0.4	12	2	12
-	Dense Grains at Reaction Zone, bulk slag in interface (not shown in Figure)	8	1	2		0.4		94	3	
Test 198 Cathode (Figure 4)										
M	Matrix		2	5		2	0.4	39	0.2	51
N	Second Phase Surrounding Matrix			34		10		6	0.1	49
O	Reaction Product in Reaction Zone	30	25	1		0.3	0.1	36	7	
P	Grain Boundary in Reaction Zone	6	28	38	9	13	0.5	0.2	3	2

The reaction product in the low iron containing slag (MR-1, test 198) consisted of 1) an oxide of Cr-Al (4:1), 2) Cr_2O_3, 3) $Y_2Si_2O_7$, and 4) slag depleted in K but containing Y and Cr.

The cathode reaction zone was different than the anode. In the high iron slag, the matrix next to the reaction zone was relatively unchanged with potassium penetration along the grain boundaries even to the platinum leadout area. The reaction zone consisted of 1) granular oxide reaction product of Al-Fe-Cr (2:3:4) and 2) slag depleted in Fe and K. In the low iron slag, the matrix grain had reacted with Si to form two compounds. 1) Y_2O_3 rich $YCrO_3$ and 2) Y_2O_3 rich $Y_2Si_2O_7$. The reaction zone consisted of a granular reaction product of Mg-Al-Cr (2:2:3) and 3) potassium depleted slag. The formation of the $Y_2Si_2O_7$ is probably enhanced by the degradation of both the anode and cathode and may be the reason for the higher corrosion rates in the MR-1 coal slag. The silicate formation may be due to the higher voltages, voltage fluctuations, or temperature excursions due to current concentrations.

In summary, yttrium chromites are potentially better MHD electrode materials than the analogous lanthanum chromites. The yttrium chromites have similar electrical and thermal properties as lanthanum chromites but yttrium chromites do not form deleterious hygroscopic compounds. The yttrium chromites are more electrochemically resistant to coal slag interactions than lanthanum chromite. Yttrium chromite is more resistant to electrochemical interactions in Ill #6 coal slag than in Montana "Rosebud" coal slag.

Rare Earth Hafnia Compositions

Several rare earth-hafnia compositions potential as high temperature MHD electrodes have been fabricated and electrochemically tested in both Montata "Rosebud" and Ill #6 slags.[9] Several of these rare earth hafnia compositions are electrochemical resistant to slag corrosion. These compounds include:

$Tb_{0.31}Hf_{0.69}O_2$

$Pr_{0.04}Tb_{0.17}Yb_{0.08}Hf_{0.71}O_2$

$Tb_{0.2}Yb_{0.1}Hf_{0.7}O_2$

$Tb_{0.18}Hf_{0.82}O_2$.

All of these materials have stabilized fluorite as the predominate crystallographic phase with small amounts of monoclinic and pyrochlore phases. (The pyrochlore phase is found in the samples containing large rare earth ions like Pr.) Electrical conductivity measurements suggest that these materials are all partially electronic and partially ionic. In general, the fluorite phase has a higher electrical conductivity than either the pyrochlore or monoclinic phase.

A series of rare earth stabilized hafnia compositions containing M_xO_y have been developed that are electronic conductors with electrical conductivities between 10^0 and 10^2 $ohm^{-1}cm^{-1}$ at room temperature and 1550K, respectively. These compositions are compatible with the rare earth-hafnia electrode materials and can be used as low temperature current leadouts. Several hafnia electrode-ceramic current leadout couples have been electrochemically tested to determine interactions between the materials. The couples consisted of rectangular paralletpipeds with the following configuration:

Pt Anode||Ceramic Current Leadout||Ceramic Electrode||Ceramic Current Leadout||Pt Cathode.

Direct electric current was passed between the two Pt wires through the ceramic couples with one current leadout-electrode interface as an anode and the other as a cathode. The tests at temperatures between 1373K and 1473K have operated for as long as 577 hrs passing 224,000 coulombs with little interaction between the leadouts and the electrodes. Further testing is continuing with a goal of producing an integrated ceramic electrode-current leadout.

Acknowledgments

The authors express appreciation to W. M. Gerry and D. I. Boget for conducting the electrochemical experiments and helping with the physical property measurements. They also thank J. L. Coleman for the SEM-EDX examination.

References

1. D. B. Meadowcroft, "Some Properties of Strontrum-doped Lanthanum Chromite." Brit. J. Appl. Phys. 2(2):1225, 1969.

2. J. B. Heywood, W. T. Norris and A. C. Warren, "Electrode and Insulation," Open-Cycle MHD Power Generation. J. B. Heywood and G. J. Womock, ed., Pergamon Press, New York, 1979.

3. H. U. Anderson, R. Murphy, K. Humphrey, B. Rossing, A. Aldred, W. L. Procarione, R. J. Ackerman and J. L. Bates, "Influence of Composition and Cation Stoichiometry on the Volatility Electrical Conductivity and Thermal Expansion of $LaCrO_3$ Based Oxides," The Rare Earth in Modern Science and Technology. G. J. McCarthy and J. J. Rhyne, ed., Plenum Press, New York, pp. 55-61, 1978.

4. J. L. Bates, "Melting Points of Hypostoichiometric Uranium Dioxide." J. Am. Cer. Soc. 49(7):395-396, 1967.

5. H. U. Anderson, R. Murphy, S. Semachaibouorn, B. Rossing, A. Aldred, W. L. Procarione and R. J. Ackermann, "Electrical Conductivity, Volatilization and Preparation of $LaCrO_3$-Based Oxides," Proceedings of Conference of High Temperature Science Related to Open Cycle, Coal-fired MHD Systems, Argonne National Laboratory, Argonne, Illinois, 1977.

6. J. L. Bates and D. D. Marchant, "Thermal Properties of MHD Electrode Materials," 17th Symposium Engineering Aspects of Magnetohydrodynamics, Palo Alto, California, 1978.

7. D. D. Marchant, C. W. Griffin and J. L. Bates, "Electrochemical Studies of MHD Channel Electrode Materials in Molten Potassium Salts and Coal Slags," 17th Symposium Engineering Aspects of Magnetohydrodynamics, Palo Alto, California, 1978.

8. J. L. Bates, D. D. Marchant, and J. L. Daniel, Development, Characterization, and Evaluation of Materials for Open Cycle MHD, PNL-2004-10, Pacific Northwest Laboratory, Richland, Washington, September 1978.

9. J. L. Bates, D. D. Marchant and J. L. Daniel, Development, Characterization, and Evaluation of Materials for Open Cycle MHD, PNL-2004-11, Pacific Northwest Laboratory, Richland, Washington, December 1978.